This article has been accepted for publication in IEEE Signal Processing Magazine. This is the author's version which has not been fully edited and content may change prior to final publication. Citation information: DOI 10.1109/MSP.2024.3384178

Augmented Statistics of Quaternion Random Variables: A Lynchpin of Quaternion Learning Machines

C. Cheong Took, S. P. Talebi, R. M. Fernandez Alcala, D. P. Mandic

I. Abstract

Learning machines for vector sensor data are naturally developed in the quaternion domain and are underpinned by quaternion statistics. To this end, we revisit the 'augmented' representation basis for discrete quaternion random variables $\mathbf{q}^a[n]$, i.e. $\left[\mathbf{q}[n] \;\; \mathbf{q}^\imath[n] \;\; \mathbf{q}^\jmath[n]\mathbf{q}^\kappa[n]\right]$; and demonstrate its pivotal role in the treatment of the generality of quaternion random variables (RV). This is achieved by a rigorous consideration of the augmented quaternion RV, and by involving for additional second order statistics, besides the traditional covariance $E\{\mathbf{q}\mathbf{q}^*\}$ [1]. To illuminate the usefulness of quaternions, we consider their most well-known application - three-dimensional (3D) orientation and offer an account of augmented statistics for purely imaginary (pure) quaternions. The quaternion statistics presented here can be exploited in the analysis of the existing and the development of novel statistical machine learning methods, hence acting as a lynchpin for quaternion learning machines.

II. Introduction

For a long time [2], quaternions were considered a niche area of research in data analytics, and even Lord Kelvin shared the same sentiment [3]:
"Quaternions came from Hamilton after his really good work had been done, and though beautifully ingenious, have been an unmixed evil to those who have touched them in any way."

In 1843, Hamilton proposed quaternions [2]. The quaternionic system was, however, challenged by the vector system proposed by Heaviside [4]. Despite the criticism, Tait continued promoting quaternions and further developed the theory of quaternions [5]. He influenced his colleague Maxwell, who simplified the well-known equations on electro-magnetism based on quaternions. Other applications of quaternions include Quantum Mechanics, Special Relativity, as well as Classical Physics [6].

The recent developments in sensor technology, such as vector sensors for wind

and speech, together with a dramatic increase in the available computing power have brought quaternions to the fore. Indeed, quaternions have been exploited in numerous *advanced* signal and information processing settings, such as in frequency analysis [7], dimension reduction [8], and hyperspectral image processing [9], as a natural domain for 3D and 4D signals. These developments have been driven by researchers such as Le Bihan, Sangwine, Valous, and Hitzer, to name but a few.

The word 'evil' according to Lord Kelvin refers, perhaps, to the fact that quaternions have been traditionally attractive mainly to researchers who are familiar with the algebra of quaternions (albeit not to many), thus giving a false impression of mathematical obscurity of quaternions [4]. This has been particularly the case with the statistics of quaternion random variables, a subject of this work. To demystify quaternion statistics to a wide research community, we here adopt a tutorial-like approach, in order to shed light onto the fundamentals of discrete quaternion statistical signal processing. Moreover, this tutorial puts quaternions into the wider context of data analytics for vector sensors by focusing on the best known application of quaternions - three-dimensional (3D) orientation or rotation - which underpins numerous real-world applications including robotics, computer vision, and virtual reality. Our aim is to demonstrate and visualise how the statistics of quaternion random variables manifest themselves in 3D and 4D. The cornerstone of this approach is the quaternion rotation, which is governed by

$$p^{\dagger}[n] = \underbrace{q[n]}_{\text{4D}} \underbrace{p[n]}_{\text{3D}} \underbrace{q^{*}[n]}_{\text{4D}} \tag{1}$$

where $p^{\dagger}[n]$ and $p[n]$ denote respectively the new and the old 3D (x, y, z) coordinate position, whereas the full 4D quaternion $q[n]$ models the 3D rotation (or orientation). The main motivations for considering quaternions $q \in \mathbb{H}$ (in the Hamiltonian quaternion space) over the real vector space $\mathbf{x} \in \mathbb{R}^3$ for 3D rotations are [10]:

1) **Discontinuities in** $\mathbb{R}^3$. The Euler angles around the $z-y-x$ axes[1] exhibit discontinuities due to the well-known phenomenon of Gimbal lock[2].

[1]In the specific order of: a rotation around the z-axis, a rotation around the y-axis, and finally a rotation around the x-axis.

[2]Gimbal lock occurs when two of the three axes of rotation collapse into one axis of rotation, leading to 2D rotation instead of 3D rotation.

2) **Smooth spherical linear interpolation in** $\mathbb{H}$. Between any two subsequent rotations it is often desired to ensure that an object is rotated smoothly in multiple smaller intermediate steps rather than in one or two larger steps. It is much more straightforward to calculate these intermediate rotations using quaternions in $\mathbb{H}$, rather than through real trivariate rotation (Euler) matrices $\mathbf{X} \in \mathbb{R}^{3\times3}$.
3) **Averaging of rotations** is widely used to mitigate noise in 3D rotation measurements from vector sensors (e.g. accelerometers and gyroscopes). Averaging over Euler's angles in $\mathbb{R}^3$ is not possible, whereas averaging rotation matrices is tedious. Yet, averaging of quaternion-based rotations is straightforward.

Due to these advantages over vectors in $\mathbb{R}^3$, quaternions have not only become the solution of choice for 3D modelling, but this is also natural, as 3D rotations and positions of variables in (1) are inherently quaternion-valued. The augmented statistical basis is crucial to exploit such quaternion operations, as explained next.

Our previous work in [1] demonstrated how the augmented basis makes it possible us to exploit different kinds of correlation, which allows for the complete order second quaternion statistics to be accounted for. In other words, the real-valued correlations of the components of a quaternion *cannot* be extracted from the quaternion-valued correlation (or covariance for zero mean data) $r_c[\ell] = \mathsf{E}\{q[n]q^*[n-\ell]\}$ alone. Indeed, the so-called complementary correlations $r_\eta[\ell] = \mathsf{E}\{q[n]q^{\eta*}[n-\ell]\}$ are also required to fully describe the second order information present in quaternions.

A. Historical perspective on quaternion statistics and machine learning

In 1999, Vakhania introduced a systemic framework for quaternion statistics in Hilbert spaces [11]. This work was followed by Amblard and Le Bihan in 2004, who examined the concept of properness[3] for quaternion random variables [12]. Via *et al.* introduced the widely linear model to exploit quaternion statistics in [13] in 2010. The following year, we showed the duality between the quaternionic and quadrivariate statistics [1]. Finally, Ginzberg and Walden looked at testing the properness of Gaus-

[3]Like in the complex domain, properness implies the rotation invariance of the probability distribution function of Gaussian variables, which is revisited in Section III-E

TABLE I: List of notations.

Notation	Name	Description or illustrative example
$\mathbb{H}$	The Hamiltonian space	Set of quaternion numbers
$\mathbb{C}$	The complex space	Set of complex numbers
$[-n]$	Time reversal	Sorting the elements of a sequence $\mathbf{q}[n]$ in a reverse order
$[n-\ell]$	Time shifting	A delay operation by ℓ samples
$\uparrow$	Time origin	The location of time index $n=0$ in a sequence $\mathbf{q}[n]$
η	Generic imaginary component	η can represent any of the imaginary units: $\imath, \jmath, \kappa$
$\Re\{\cdot\}$	Real component	$q_s[n]$
$\Im_\eta\{\cdot\}$	η-imaginary component	$q_x[n]$ (if $\eta=\imath$)
$\Im_\alpha\{\cdot\}$	α-imaginary component where $\alpha \neq \eta$	$q_y[n]$ or $q_z[n]$ (if $\eta=\imath$)
$(\cdot)^*$	Conjugation	$q_s[n]-q_x[n]\imath-q_y[n]\jmath-q_z[n]\kappa$
$(\cdot)^\eta$	η-imaginary involution	$q_s[n]-q_x[n]\imath-q_y[n]\jmath+q_z[n]\kappa$ (if $\eta=\kappa$). See Eq. (9) for more details.
$(\cdot)^{\mathsf{H}}$	Hermitian operator	$(\cdot)^*$ followed by transpose $(\cdot)^{\mathsf{T}}$ (or vice versa)
$(\cdot)^{\eta\mathsf{H}}$	η-Hermitian operator [19]	$(\cdot)^\eta$ followed by $(\cdot)^{\mathsf{H}}$ (or vice versa)
$\mathsf{E}\{\cdot\}$	Statistical expectation operator	Calculates the expected value on 'average'
$r[\ell]$	Quaternion autocorrelation	Quaternion-valued autocorrelation at lag ℓ
$c_{ij}[\ell]$	Real Autocorrelation	Real auto-correlation between ith and jth channel
$\mathbf{R}[n]$	Quaternion correlation matrix	Quaternion correlation matrix at time n, e.g. see Eq. (29).
$\mathbf{\Lambda}$	Lambda matrix	A matrix with a diagonal structure
$\perp$	Perpendicular	Orthogonality between two variables
$\cdot$	Inner product	See Eq. (4) for quaternion product
$\times$	Outer product	See Eq. (5) for quaternion product
Toep$\{\mathbf{x}[n]\}$	Toeplitz matrix	Construct a Toeplitz matrix using vector $\mathbf{x}[n]$

sian random variables [14]. For a more complete overview of quaternion statistics, readers are referred to [12]. Since then, augmented statistics for quaternions have become a lynchpin for numerous statistical machine learning algorithms in $\mathbb{H}$, such as variational auto-encoders [15], generative adversarial networks [16], and kernel learning [17]. We refer to a survey on quaternion neural networks in [18] for additional quaternion-valued machine learning methods.

B. Notations

Table I summarises the notations employed in this work and in our sister paper [20]. In the context of a quaternion depicting a 3D position, as in Eq. (1), the imaginary components (or vector part) correspond to the (x, y, z) coordinates with the real (or

scalar) part $q_s[n] = 0$. Scalar quaternion values are denoted by italics, $q[n]$, vectors are denoted by lowercase bold font, $\mathbf{q}[n]$, and matrices by bold uppercase bold letters, $\mathbf{Q}[n]$. Sets are generally denoted by capital letters in calligraphic font such as $\mathcal{Q}[n]$.

C. Basics of quaternions

As quaternions are hypercomplex numbers, they are comprised of a scalar (real) part and a vector part made up of three imaginary parts. In other words, a quaternion variable $q[n]$ can be expanded component-wise, as

$$q[n] \;=\; q_s[n] + q_x[n]\imath + q_y[n]\jmath + q_z[n]\kappa \tag{2}$$

where the real part is $\Re\{q[n]\} = q_s[n]$ and its vector part is made up of three imaginary components, i.e. $\Im\{q[n]\} = q_x[n]\imath + q_y[n]\jmath + q_z[n]\kappa$. These imaginary units obey the following rules

$$\imath^2 = \jmath^2 = \kappa^2 = -1, \qquad \imath\jmath = \kappa, \qquad \jmath\kappa = \imath, \quad \kappa\imath = \jmath \tag{3}$$

A quaternion product between $q_1[n]$ and $q_2[n]$ can be computed as

$$\Re\{q_1[n]q_2[n]\} \;=\; \Re\{q_1[n]\}\Re\{q_2[n]\} - \Im\{q_1[n]\} \cdot \Im\{q_2[n]\} \tag{4}$$

$$\Im\{q_1[n]q_2[n]\} \;=\; \Re\{q_1[n]\}\Im\{q_2[n]\} + \Re\{q_2[n]\}\Im\{q_1[n]\} + \Im\{q_1[n]\} \times \Im\{q_2[n]\} \tag{5}$$

Observe the outer product '$\times$' in Eq. (5) implies the noncommutativity of the quaternion product. On the other hand, the inner product '$\cdot$' between the two vector parts in Eq. (4) guarantees that the product of the real parts remains a scalar. A consequence of the noncommutativity of the quaternion product implies the following, in contrast to Eq. (3)

$$\jmath\imath = -\kappa, \qquad \kappa\jmath = -\imath, \quad \imath\kappa = -\jmath \tag{6}$$

Like a complex number, a quaternion can be conjugated by negating its imaginary parts, that is

$$q^*[n] = q_s[n] - q_x[n]\imath - q_y[n]\jmath - q_z[n]\kappa \tag{7}$$

The conjugate can be used to calculate the inverse of a quaternion $q^{-1}[n] = \frac{q^*[n]}{\|q[n]\|}$, whereby the norm $\|q[n]\|$ is given by

$$\begin{aligned} \|q[n]\| &= \sqrt{q[n]q^*[n]} \\ &= \sqrt{q_s^2[n] + q_x^2[n] + q_y^2[n] + q_z^2[n]} \end{aligned} \tag{8}$$

This norm is useful in normalising quaternions into unit quaternions $q[n] = q[n]/\|q[n]\|$, which are used in 3D rotations. In other words, in Eq. (1) the norm of the rotation quaternion $\|q[n]\| = 1$. Next, the algebra of quaternions based on involutions is revisited for background purposes of this tutorial.

D. Quaternion Algebra based on Involutions

Open literature treats extensively and rigorously quaternion algebra, such as the work by Voight [21]. The aim of this section is to focus on the so called quaternion 'involutions' and to present their algebraic properties in an accessible way. The basics of univariate quaternion algebra required for this tutorial are covered, while a more comprehensive review is provided in our sister paper [20]. This section concludes by revisiting some properties of quaternion matrices and is based on our previous work [19].

As shown in Eq. (7), the quaternion conjugate, like with the complex numbers, can be obtained as $q^*[n] = \Re\{q[n]\} - \Im\{q[n]\}$, which also represents the quaternion inverse $q^{-1}[n] = q^*[n]$, provided $q[n]$ has a unit norm.

Similarly, an involution represents a self-inverse mapping, e.g. $(q^*[n])^* = q[n]$. In the context of this work, however, we treat quaternion involutions as the three perpendicular involutions, given by

$$\begin{aligned} &q^{\imath}[n] = q_s[n] + \imath q_x[n] - \jmath q_y[n] - \kappa q_z[n] \qquad q^{\jmath}[n] = q_s[n] - \imath q_x[n] + \jmath q_y[n] - \kappa q_z[n] \\ &q^{\kappa}[n] = q_s[n] - \imath q_x[n] - \jmath q_y[n] + \kappa q_z[n] \end{aligned} \tag{9}$$

In other words, for any $\eta-$involution, the operation $q^{\eta}[n] = -\eta q[n]\eta$ conjugates all imaginary components except for the imaginary η-component. These quaternion

involutions obey the following algebraic rules

$$\begin{aligned} (q^*[n])^\eta &= (q^\eta[n])^* \qquad (p[n]+q[n])^\eta = p^\eta[n]+q^\eta[n] \\ (p[n]q[n])^\eta &= p^\eta[n]q^\eta[n] \qquad (p[n]q[n])^{\eta*} = q^{\eta*}[n]p^{\eta*}[n] \\ (p^\alpha[n])^\eta &= (p^\eta[n])^\alpha = p^\delta \qquad \forall \eta \neq \alpha \neq \delta \in \{\imath, \jmath, \kappa\} \end{aligned} \tag{10}$$

The quaternion involutions can be manipulated matrix-wise as

$$\begin{aligned} (\mathbf{Q}^*[n])^\mathsf{T} = (\mathbf{Q}^\mathsf{T}[n])^* = \mathbf{Q}^\mathsf{H}[n] \qquad & (\mathbf{P}[n]\mathbf{Q}[n])^* \neq \mathbf{P}^*[n]\mathbf{Q}^*[n] \\ (\mathbf{Q}^*[n])^\eta = (\mathbf{Q}^\eta[n])^* \qquad & (\mathbf{P}[n]\mathbf{Q}[n])^\mathsf{T} \neq \mathbf{Q}^\mathsf{T}[n]\mathbf{P}^\mathsf{T}[n] \\ (\mathbf{Q}^\eta[n])^\mathsf{T} = (\mathbf{Q}^\mathsf{T}[n])^\eta \qquad & (\mathbf{P}[n]\mathbf{Q}[n])^\eta = \mathbf{P}^\eta[n]\mathbf{Q}^\eta[n] \\ (\mathbf{Q}^\eta[n])^\mathsf{H} = (\mathbf{Q}^\mathsf{H}[n])^\eta \qquad & (\mathbf{P}[n]\mathbf{Q}[n])^\mathsf{H} = \mathbf{Q}^\mathsf{H}[n]\mathbf{P}^\mathsf{H}[n] \\ (\mathbf{Q}^\delta[n])^\eta = (\mathbf{Q}^\eta[n])^\delta = \mathbf{Q}^\alpha[n] \qquad & (\mathbf{P}[n]\mathbf{Q}[n])^{\eta\mathsf{H}} = \mathbf{Q}^{\eta\mathsf{H}}[n]\mathbf{P}^{\eta\mathsf{H}}[n] \\ & \forall \eta \neq \delta \neq \alpha \in \{\imath, \jmath, \kappa\} \end{aligned} \tag{11}$$

For clarity and conciseness, these equations are stated without proofs, however, the curious reader is referred to our previous work [19] for more details. Our sister paper [20] demonstrates how the augmented statistics (via the augmented basis) can act as a lynchpin for learning machines on quaternion data. This work, however, introduces augmented quaternion statistics via numerical examples and 3D orientation applications. This approach is different from our previous work [1] on augmented statistics in two ways. First, the current work is presented as a tutorial with numerical examples. Second, this tutorial illustrates quaternion statistics via 3D orientation examples, while our previous work [1] focused on the mapping between quaternion-valued covariances and their real-valued counterparts to illustrate quaternion statistics.

III. The Augmented Basis in $\mathbb{H}$

Given that digital signal processing (DSP) relies on several basic operations, such as time reversal and time-shifting, we present for the first time their relevance for quaternion-valued sequences, their characterisation, and their statistics.

This article has been accepted for publication in IEEE Signal Processing Magazine. This is the author's version which has not been fully edited and content may change prior to final publication. Citation information: DOI 10.1109/MSP.2024.3384178

A. Significance of the augmented basis

A quaternion variable, $q[n]$, depends intrinsically on its involutions and their conjugates, as

$$q[n] \;=\; \frac{1}{2}(q^{\imath *}[n] + q^{\jmath *}[n] + q^{\kappa *}[n] - q^{*}[n]) \tag{12}$$

so that, unlike complex numbers, it is not possible to extract algebraically each component of a quaternion variable, i.e. $q_s[n], q_x[n], q_y[n], q_z[n]$ using only the variable $q[n]$ and its conjugate. Indeed, the calculations of these components *require* both the quaternion involutions and conjugate operations, in the form

$$q_s[n] = \frac{1}{2}(q[n] + q^{*}[n]) \qquad q_y[n] = \frac{1}{2\jmath}(q[n] - q^{\jmath *}[n])$$
$$q_x[n] = \frac{1}{2\imath}(q[n] - q^{\imath *}[n]) \qquad q_z[n] = \frac{1}{2\kappa}(q[n] - q^{\kappa *}[n])$$

This exemplifies the significance of quaternion involutions, which are used to construct the only general quaternion representation basis, which extends from the original quaternion, $q[n]$, to its augmented counterpart $\Big[q[n],\ q^{\imath}[n],\ q^{\jmath}[n],\ q^{\kappa}[n]\Big]$, as considered in our sister paper [20].

B. Characterisation of discrete quaternion sequences

A sequence $\mathbf{q}[n]$ is called a conjugate symmetric sequence if $\mathbf{q}[n] = \mathbf{q}^{*}[-n]$, whereby the negative sign designates the key DSP operation of time reversal. In the same spirit, we can now define such sequences based on quaternion involutions. A sequence is called a conjugate η-symmetric sequence, $\mathbf{q}_{\eta s}[n]$, if

$$\mathbf{q}[n] = \mathbf{q}^{\eta *}[-n] \quad \eta \in \{\imath, \jmath, \kappa\} \tag{13}$$

In other words, the η-imaginary components are conjugates of each other at the time indices n and $-n$, whereas the other α-imaginary components are not necessarily so when $\alpha \neq \eta$. Notice that Eq. (13) implies that at the time origin, $n = 0$, the corresponding imaginary component vanishes, i.e. $\Im_{\eta}\{\mathbf{q}[0]\} = 0$. On the other hand,

a conjugate anti η-symmetric sequence, $\mathbf{q}_{\eta a}[n]$, satisfies

$$\mathbf{q}[n] = -\mathbf{q}^{\eta *}[-n] \quad \eta \in \{\imath, \jmath, \kappa\} \tag{14}$$

Essentially, Eq. (14) means that $\mathbf{q}[n] = -\mathbf{q}[-n]$ except for the η-imaginary component, since $\Im_\eta\{\mathbf{q}[n]\} = \Im_\eta\{\mathbf{q}[-n]\}$. In contrast to Eq. (13), the $\eta-$imaginary component does not vanish, $\Im_\eta\{\mathbf{q}[0]\} \neq 0$, at the time index $n = 0$, but the other components vanish, i.e. $\Re\{\mathbf{q}[0]\} = \Im_\alpha\{\mathbf{q}[0]\} = 0$, where $\alpha \neq \eta$. The so-defined sequences can be used to construct the original quaternion sequence (and vice-versa) as

$$\mathbf{q}[n] = \mathbf{q}_{\eta s}[n] + \mathbf{q}_{\eta a}[n] \tag{15}$$

$$\mathbf{q}_{\eta s}[n] = \frac{1}{2}\big(\mathbf{q}[n] + \mathbf{q}^{\eta *}[-n]\big) \tag{16}$$

$$\mathbf{q}_{\eta a}[n] = \frac{1}{2}\big(\mathbf{q}[n] - \mathbf{q}^{\eta *}[-n]\big) \tag{17}$$

These newly characterised quaternion sequences can be used to construct the accurate descriptors of second order correlations. This is further illustrated in Example 1 which gives a numerical demonstration of a conjugate $\imath$-symmetric sequence in Eq. (24) and its anti-symmetric counterpart in Eq. (25).

C. Second order statistics of 'full' quaternion random variables.

For simplicity and without loss of generality, we assume that all random processes considered have zero mean, so all the correlation measures in this work are equal to their covariance counterparts. The characteristic autocorrelation sequences of $\mathbf{q}[n]$, the building blocks for the second order autocorrelation matrices, are defined[4] as

$$r_c[\ell] = \sum_{n=-\infty}^{n=\infty} q[n]q^*[n-\ell] \tag{18}$$

$$r_p[\ell] = \sum_{n=-\infty}^{n=\infty} q[n]q[n-\ell] \tag{19}$$

$$r_\eta[\ell] = \sum_{n=-\infty}^{n=\infty} q[n]q^{\eta *}[n-\ell] \tag{20}$$

[4]These autocorrelations can be normalised by the number of samples in a signal, as considered in the simulations.

This article has been accepted for publication in IEEE Signal Processing Magazine. This is the author's version which has not been fully edited and content may change prior to final publication. Citation information: DOI 10.1109/MSP.2024.3384178

EXAMPLE 1. Consider the sequence $\mathbf{q}[n]$ which is defined for $-2 \leq n \leq 2$ as

$$\mathbf{q}[n] = \Big[1{+}4\imath{+}\jmath{+}\kappa,\ -2{+}3\imath{+}2\jmath{+}2\kappa,\ \underset{\uparrow}{4-2\imath+3\jmath+3\kappa},\ -5{-}6\imath{+}4\jmath{+}4\kappa,\ -3{-}2\imath{+}5\jmath{+}5\kappa\Big] \quad (21)$$

To determine its conjugate $\imath-$symmetric part, $\mathbf{q}_{\imath s}[n]$, it is first $\imath$-conjugated as

$$\mathbf{q}^{\imath*}[n] = \Big[1{-}4\imath{+}\jmath{+}\kappa,\ -2{-}3\imath{+}2\jmath{+}2\kappa,\ \underset{\uparrow}{4+2\imath+3\jmath+3\kappa},\ -5{+}6\imath{+}4\jmath{+}4\kappa,\ -3{+}2\imath{+}5\jmath{+}5\kappa\Big] \quad (22)$$

and then time-reversed to yield

$$\mathbf{q}^{\imath*}[-n] = \Big[-3{+}2\imath{+}5\jmath{+}5\kappa\ -5{+}6\imath{+}4\jmath{+}4\kappa,\ \underset{\uparrow}{4+2\imath+3\jmath+3\kappa},\ -2{-}3\imath{+}2\jmath{+}2\kappa,\ 1{-}4\imath{+}\jmath{+}\kappa\Big] \quad (23)$$

Upon substituting Eq. (21) and Eq. (23) into Eq. (16), the conjugate $\imath-$symmetric part $\mathbf{q}_{\imath s}[n]$ can be obtained as

$$\mathbf{q}_{\imath s}[n] = \Big[-1{+}3\imath{+}3\jmath{+}3\kappa,\ -3.5{+}4.5\imath{+}3\jmath{+}3\kappa,\ \underset{\uparrow}{4+3\jmath+3\kappa},\ -3.5{-}4.5\imath{+}3\jmath{+}3\kappa,\ -1{-}3\imath{+}3\jmath{+}3\kappa\Big] \quad (24)$$

Likewise, Eq. (17) can be used to compute its conjugate anti $\imath$-symmetric sequence, $\mathbf{q}_{\imath a}[n]$, as

$$\mathbf{q}_{\imath a}[n] = \Big[2+\imath-2\jmath-2\kappa,\ 1.5-1.5\imath-\jmath-\kappa,\ \underset{\uparrow}{-2\imath},\ -1.5-1.5\imath+\jmath+\kappa,\ -2+\imath+2\jmath+2\kappa\Big] \quad (25)$$

Observe in Eq. (24) the vanishing $\imath$-component of the element $\Im_\imath\{q_{\imath s}[0]\} = 0$ at time index $n = 0$, in contrast to that in Eq. (25). Adding both elements at $n = 0$ gives back $q[0] = 4 - 2\imath + 3\jmath + 3\kappa$ in Eq. (21).

It is straightforward to see from Eq. (12) that the relationship between the auto-correlation measures in Eqs. (18)-(20) is given by

$$r_p[\ell] \ = \ \frac{1}{2}\Big(r_\imath[\ell] + r_\jmath[\ell] + r_\kappa[\ell] - r_c[\ell]\Big) \quad (26)$$

Eq. (26) implies that knowing any four of these five autocorrelation descriptors is *sufficient* to determine the fifth unknown autocorrelation. In other words, only four of these five autocorrelations are *sufficient* to capture the second order information of the signal. These autocorrelations have the following properties:

P1. $r_c[\ell]$ are conjugate symmetric, i.e. $r_c[\ell] = r_c^*[-\ell]$,

P2. $r_c[\ell]$ attains its maximum at $\ell = 0$, i.e. $r_c[0] \geq r_c[\ell]\ \forall \ell \neq 0$,

P3. $r_\eta[\ell]$ are conjugate η-symmetric, i.e. $r_\eta[\ell] = r_\eta^{\eta*}[-\ell]$,

P4. All autocorrelations $r[\ell]$ are symmetric in terms of the absolute magnitude, i.e. $|r[\ell]| = |r[-\ell]|$.

Notice that $r_p[\ell]$ does not exhibit a symmetry analogous to Properties P1 and P3, due to the non-commutativity of the quaternion product. Still, Property P4 means that $r_p[\ell]$ is symmetric in terms of its absolute magnitude, i.e. $|r_p[\ell]| = |r_p[-\ell]|$. These correlation sequences are important building blocks to characterise the second order information of discrete-time random processes in the matrix form. For instance, $r_\eta[\ell]$ can be used to construct the complementary $\eta-$correlation matrix $\mathsf{E}\{\mathbf{q}[n]\mathbf{q}^{\eta\mathsf{H}}[n]\}$. For further illustration, consider the vector

$$\mathbf{q}[n] = \Big[q[n], q[n-1], \ldots, q[n-\tau]\Big]^{\mathsf{T}} \tag{27}$$

of τ quaternion values. Then, its outer product is given by

$$\mathbf{q}[n]\mathbf{q}^{\eta\mathsf{H}}[n] = \begin{bmatrix} q[n]q^{\eta*}[n] & q[n]q^{\eta*}[n-1] & \cdots & q[n]q^{\eta*}[n-\tau] \\ q[n-1]q^{\eta*}[n] & q[n-1]q^{\eta*}[n-1] & \cdots & q[n-1]q^{\eta*}[n-\tau] \\ \vdots & \vdots & \ddots & \vdots \\ q[n-\tau]q^{\eta*}[n] & q[n-\tau]q^{\eta*}[n-1] & \cdots & q[n-\tau]q^{\eta*}[n-\tau] \end{bmatrix} \tag{28}$$

which is a $\tau \times \tau$ matrix. Taking its expected value yields the η-autocorrelation matrix

$$\mathbf{R}_\eta[n] = \begin{bmatrix} r_\eta[0] & r_\eta[1] & \cdots & r_\eta[\tau] \\ r_\eta[-1] & r_\eta[0] & \cdots & r_\eta[\tau-1] \\ \vdots & \vdots & \ddots & \vdots \\ r_\eta[-\tau] & r_\eta[1-\tau] & \cdots & r_\eta[0] \end{bmatrix} = \begin{bmatrix} r_\eta[0] & r_\eta[1] & \cdots & r_\eta[\tau] \\ r_\eta^{\eta*}[1] & r_\eta[0] & \cdots & r_\eta[\tau-1] \\ \vdots & \vdots & \ddots & \vdots \\ r_\eta^{\eta*}[\tau] & r_\eta^{\eta*}[\tau-1] & \cdots & r_\eta[0] \end{bmatrix} \tag{29}$$

Similarly, the autocorrelation matrices $\mathbf{R}_c[n] = \mathsf{E}\{\mathbf{q}[n]\mathbf{q}^{\mathsf{H}}[n]\}$ and $\mathbf{R}_p[n] = \mathsf{E}\{\mathbf{q}[n]\mathbf{q}^{\mathsf{T}}[n]\}$ are made up respectively of $r_c[\ell]$ and $r_p[\ell]$. Such an η-correlation matrix has the following properties:

PI. The η-autocorrelation matrix has an η-Hermitian Toeplitz structure due to Prop-

erty P3, that is

$$\mathbf{R}_{\eta}[n] = \text{Toep}\{r_{\eta}[0], r_{\eta}[1], \ldots, r_{\eta}[\tau]\} \tag{30}$$

PII. The η-autocorrelation matrix can be factorised as [19]

$$\mathbf{R}_{\eta}[n] = \mathbf{\Phi}\mathbf{\Lambda}_s\mathbf{\Phi}^{\eta\mathsf{H}} \tag{31}$$

where $\mathbf{\Lambda}_s$ is a diagonal matrix of the singular values of $\mathbf{R}_{\eta}[n]$, and $\mathbf{\Phi}$ is a unitary matrix. The diagonalisation in Eq. (31) is useful in testing the degree of properness of quaternions, which is discussed in Section III-E,

PIII. The η-autocorrelation matrix $\mathbf{R}_{\eta}[n]$ can be diagonalised simultaneously with the autocorrelation matrix $\mathbf{R}_{c}[n]$ as [22]

$$\mathbf{\Psi}\mathbf{R}_{c}[n]\mathbf{\Psi}^{H} = \mathbf{\Lambda}_a \qquad \mathbf{\Psi}\mathbf{R}_{\eta}[n]\mathbf{\Psi}^{\eta H} = \mathbf{\Lambda}_b \tag{32}$$

where $\mathbf{\Lambda}_a = \mathbf{I}$ is an identity matrix and $\mathbf{\Lambda}_b$ is a diagonal matrix with non-negative real values. This is known as the quaternion strong uncorrelating transform (QSUT) [22]. The QSUT has been exploited in the classification of electroencephalogram (EEG) data [23], while its approximate but computationally efficient counterpart AUT (approximate uncorrelating transform) has been used in the convergence analysis of adaptive filters [24].

To facilitate the adoption of Properties PII in Eq. (31) and PIII in Eq. (32) in practical applications, their pseudo-codes are listed below.

PSEUDOCODE 1. Computation of $\mathbf{\Phi}$ in Property PII in Eq. (31).

1. Compute $\mathbf{\Lambda}_s$ using singular value decomposition (SVD)

$\mathbf{R}_{\eta}[n] = \mathbf{U}_s\mathbf{\Lambda}_s\mathbf{V}_s^{\mathsf{H}}$

2. Compute the unitary matrix $\mathbf{\Phi}$

$\mathbf{\Phi} = \mathbf{U}_s(\mathbf{D}^{\eta})^{1/2}$, where $\mathbf{D} = \mathbf{V}_s^{\eta\mathsf{H}}\mathbf{U}_s$

This article has been accepted for publication in IEEE Signal Processing Magazine. This is the author's version which has not been fully edited and content may change prior to final publication. Citation information: DOI 10.1109/MSP.2024.3384178

PSEUDOCODE 2. Computation of $\mathbf{\Psi}$ in Property PIII in Eq. (32).

1. Calculate the SVD of $\mathbf{R}_c[n]$ as

$\mathbf{R}_c[n] = \mathbf{U}_c \mathbf{\Lambda}_c \mathbf{U}_c^{\mathsf{H}}$

2. Compute the whitening matrix $\mathbf{W}$

$\mathbf{W} = (\mathbf{\Lambda}_c)^{-1/2} \mathbf{U}_c^{\mathsf{H}}$

3. Apply $\mathbf{W}$ to the η-correlation matrix $\mathbf{R}_\eta[n]$ as

$\mathbf{W}\mathbf{R}_\eta[n]\mathbf{W}^{\eta\mathsf{H}} = \mathbf{\Gamma}$

4. Factorise $\mathbf{\Gamma}$ using **PSEUDOCODE 1** to compute $\mathbf{\Phi}$

$\mathbf{\Gamma} = \mathbf{\Phi}\mathbf{\Lambda}_s\mathbf{\Phi}^{\eta\mathsf{H}}$

5. Compute $\mathbf{\Psi}$ using results from Step 2 and Step 4

$\mathbf{\Psi} = \mathbf{\Phi}^{\mathsf{H}}\mathbf{W}$

Both **PSEUDOCODE**[5] **1** and **2** require the computation of quaternion SVD, which is readily available from the quaternion Matlab toolbox [25]. For clarity, Example 2 provides a numerical illustration[6] of the diagonalisation of the $\imath$-autocorrelation based on **PSEUDOCODE 1**, whereas **PSEUDOCODE 2** represents essentially the traditional pre-whitening process followed by **PSEUDOCODE 1**.

[5]The Matlab implementation for **PSEUDOCODE 1** is available here, whereas that of **PSEUDOCODE 2** can be downloaded here.

[6]All numerical values are presented to an accuracy of 2 decimal places and time indexing $[n]$ is dropped due to limited space.

This article has been accepted for publication in IEEE Signal Processing Magazine. This is the author's version which has not been fully edited and content may change prior to final publication. Citation information: DOI 10.1109/MSP.2024.3384178

EXAMPLE 2. Consider the factorisation of the $\imath$-autocorrelation matrix $\mathbf{R}_\imath = \mathbf{\Phi}\mathbf{\Lambda}_s\mathbf{\Phi}^{\imath\mathsf{H}}$, which is listed in **PSEUDOCODE 1** and is given by

$$\mathbf{R}_\imath = \begin{bmatrix} 19.62 - 13.67\jmath + 13.52\kappa & 19.68 - 0.03\imath - 13.70\jmath + 13.57\kappa \\ 19.68 + 0.03\imath - 13.70\jmath + 13.57\kappa & 19.62 - 13.67\jmath + 13.52\kappa \end{bmatrix} \quad (\times 10^{-2})$$

Observe that each row of the matrix is derived from a conjugate $\imath-$symmetric sequence $\big[r_\imath[-\ell], \ldots, r_\imath[0], \ldots, r_\imath[\ell]\big]$, with the diagonal elements as $r_\imath[0]$. As such, its diagonal elements have vanishing $\imath-$components and its off-diagonals have conjugate $\imath-$components. This ensures the $\imath-$Hermitian property of $\mathbf{R}_\imath = \mathbf{R}_\imath^{\imath\mathsf{H}}$. Its two singular values are $\lambda_1 = 0.55$ and $\lambda_2 = 7.48 \times 10^{-4}$ and the unitary matrices $\mathbf{U}_s$ and $\mathbf{V}_s$ can be obtained using SVD as

$$\mathbf{U}_s = \begin{bmatrix} 0.51 - 0.35\jmath + 0.35\kappa & 0.53 - 0.21\jmath + 0.42\kappa \\ 0.51 - 0.35\jmath + 0.35\kappa & -0.53 + 0.21\jmath - 0.42\kappa \end{bmatrix}$$

$$\mathbf{V}_s = \begin{bmatrix} 0.71 & -0.71 \\ 0.71 & 0.71 \end{bmatrix}$$

Prior to the computation of $\mathbf{\Phi}$, the diagonal matrix $\mathbf{D}$ is obtained as[a]

$$\mathbf{D} = \mathbf{V}_s^{\imath\mathsf{H}}\mathbf{U}_s = \begin{bmatrix} 0.71 - 0.50\jmath + 0.49\kappa & 0 \\ 0 & -0.75 + 0.30\jmath - 0.59\kappa \end{bmatrix}$$

Finally, the unitary matrix $\mathbf{\Phi}$ can be computed as

$$\mathbf{\Phi} = \mathbf{U}_s(\mathbf{D}^\imath)^{1/2} = \begin{bmatrix} 0.65 - 0.19\jmath + 0.19\kappa & -0.25 - 0.30\jmath + 0.59\kappa \\ 0.65 - 0.19\jmath + 0.19\kappa & 0.25 + 0.30\jmath - 0.59\kappa \end{bmatrix}$$

where $(\mathbf{D}^\imath)^{1/2}$ can be expressed as

$$(\mathbf{D}^\imath)^{1/2} = \begin{bmatrix} (0.71 + 0.50\jmath - 0.49\kappa)^{0.5} & 0 \\ 0 & (-0.75 - 0.30\jmath + 0.59\kappa)^{0.5} \end{bmatrix}$$

Hence, the $\imath-$autocorrelation $\mathbf{R}_\imath$ can be diagonalised as

$$\mathbf{\Phi}^{\mathsf{H}}\mathbf{R}_\imath\mathbf{\Phi}^\imath = \mathbf{\Lambda}_s = \begin{bmatrix} 0.55 & 0 \\ 0 & 7.48 \times 10^{-4} \end{bmatrix}$$

[a]Note that $\mathbf{V}_s^{\imath\mathsf{H}} = \mathbf{V}_s^{\mathsf{T}}$, since $\mathbf{V}_s$ is real-valued in this example.

D. Simplification of second order statistics for 'degenerate' quaternion random variables

There are many instances when full quaternion modelling is not required, and degenerate cases[7] are adequate for engineering applications, as in the modelling of three dimensional (3D) coordinates on a sphere or 2D coordinates for modelling horizontal motion. These degenerate cases of quaternion modelling can simplify its statistics (and computation), which is addressed next.

Degenerate quaternions for 3D. Pure quaternions take the form $p[n] = p_x[n]\imath + p_y[n]\jmath + p_z[n]\kappa$, and can be used for modelling 3D trajectories, whereby they represent the 'position' variable $p[n]$ in Eq. (1). In the context of pure quaternions, the pseudo-autocorrelation $r_p[\ell]$ and the autocorrelation $r_c[\ell]$ are related as[8]

$$r_p[\ell] \;\; = \;\; -r_c[\ell] \tag{33}$$

which implies that Eq. (26) becomes

$$r_c[\ell] \;\; = \;\; -\Big(r_\imath[\ell] + r_\jmath[\ell] + r_\kappa[\ell] \Big) \tag{34}$$

Hence, Eq. (34) implies that, for pure quaternions, only three correlation descriptors are sufficient to capture the complete second order statistics. This is a reduction from the requirement of having four known descriptors, as in Eq. (26) for full quaternions.

Degenerate quaternions for 2D modelling. Any two out of the three imaginary components can be used for such modelling, as in Table II which shows which of those two imaginary units are considered to design a particular 2D trajectory. In addition, its last two columns show that only two correlation measures are sufficient, although this pair of correlation measures cannot be selected arbitrarily.

TABLE II: Relationships between autocorrelations for 2D quaternion modelling.

Modelling	Application	Relationship I	Relationship II
$p[n] = p_x[n]\imath + p_y[n]\jmath$	2D horizontal trajectory	$r_\imath[\ell] = -r_\jmath[\ell]$	$r_\kappa[\ell] = -r_c[\ell]$
$p[n] = p_x[n]\imath + p_z[n]\kappa$	2D vertical trajectory in X plane	$r_\imath[\ell] = -r_\kappa[\ell]$	$r_\jmath[\ell] = -r_c[\ell]$
$p[n] = q_y[n]\jmath + p_z[n]\kappa$	2D vertical trajectory in Y plane	$r_\jmath[\ell] = -r_\kappa[\ell]$	$r_\imath[\ell] = -r_c[\ell]$

[7]The term 'degenerate' means that the quaternion is not full.

[8]For pure quaternions p and q, Eq. (33) can be verified by the quaternion product equivalence $pq = -pq^*$.

For example, when considering the 2D horizontal trajectory, only $r_\imath[\ell]$ or $r_\jmath[\ell]$ and $r_c[\ell]$ or $r_p[\ell]$ or $r_\kappa[\ell]$ are sufficient. If we consider $r_\imath[\ell]$ and $r_c[\ell]$, then Eq. (34) confirms the relationships in Table II, given by

$$\begin{aligned} r_c[\ell] &= -\Big(r_\imath[\ell] + r_\jmath[\ell] - r_c[\ell]\Big) \\ r_\imath[\ell] &= -r_\jmath[\ell] \end{aligned} \tag{35}$$

and

$$\begin{aligned} r_c[\ell] &= -\Big(r_\imath[\ell] - r_\imath[\ell] + r_\kappa[\ell]\Big) \\ r_c[\ell] &= -r_\kappa[\ell] \end{aligned} \tag{36}$$

Remark 1. The degeneracy of a particular axis (i.e. zero values along that axis) implies its redundancy in the quaternion statistics of a problem in hand. Consequently, the corresponding autocorrelation is also redundant since $r_\eta[\ell] = r_p[\ell] = -r_c[\ell]$. For example, in a 2D vertical trajectory in the Y plane, there is no activity along the x-axis, leading the redundancy of $r_\imath[\ell] = r_p[\ell]$.

Remark 2. The dependency of two axes (i.e. non-zero values along these two axes) can be captured by either of the corresponding autocorrelations. For instance, in a horizontal trajectory, the dependency between the x and y axes can be seen from $r_\imath[\ell] = -r_\jmath[\ell]$.

Remark 3. The redundancy in statistics is useful to compute a more accurate estimate of the statistical correlations. For instance in a 2D horizontal trajectory, we have $r_c[\ell] = -r_\kappa[\ell]$. Computing both $r_c[\ell]$ and $r_\kappa[\ell]$ would be redundant, yet computing both autocorrelations separately from the data and their 'averaging' would ensure a more accurate estimate of the two correlation measures in practice, especially for noisy signals. As such, for robustness against noise, the corresponding vector augmentation in the X-Y plane would be $\mathbf{q}^a[n] = \Big[\mathbf{q}[n]\ \mathbf{q}^\kappa[n]\Big]$ for 2D proper signals.

Difference from $\mathbb{C}$ for 2D modelling. It is instructive to illustrate how the 2D modelling via quaternions would differ, if the complex domain $\mathbb{C}$ was considered instead. First, the $\mathbb{C}$ modelling would require the use of the real part of the complex numbers, unlike in Table II which requires only the imaginary parts of a quater-

nion. This fundamental difference leads to the following deviations from quaternion statistics:

1) The relationship between the pseudo-autocorrelation $r_p[\ell]$ and the autocorrelation $r_c[n]$ in Eq. (33) no longer holds. The only possible way for these to share a relationship (i.e. equality), is if 2D degnerates into 1D.
2) There is no relationship between the pseudo-autocorrelation $r_p[\ell]$ and the η-autocorrelation $r_\eta[n]$ in $\mathbb{C}$, whereas it can be shown that there can be a relationship between pseudo-autocorrelation $r_p[\ell]$ and the η-autocorrelation $r_\eta[\ell]$ in $\mathbb{H}$ by making use of Eq. (33), i.e. substitute $r_c[\ell]$ with $r_p[\ell]$ in Table II.
3) The pseudo-autocorrelation $r_p[\ell]$ does exhibit the symmetry $r_p[\ell] = r_p[-\ell]$ in $\mathbb{C}$, unlike in $\mathbb{H}$. This is due to the commutativity of the complex product.

The second order statistics of quaternions would not be complete if the concept of properness is not revisited, the subject of the next section.

E. Properness in $\mathbb{H}$

There are several theoretical definitions for this second-order statistical property in the literature. For example, $\mathbb{Q}-$properness describes a quaternion random variable with three vanishing complementary covariances (i.e. $\mathbf{R}_\imath = \mathbf{R}_\jmath = \mathbf{R}_\kappa = \mathbf{0}$); $\mathbb{C}-$properness means two of the three complementary covariances vanish; and finally $\mathbb{R}-$properness implies only one of the three complementary covariances is zero [13]. On the other hand, a Gaussian quaternion random variable is called $(\eta, \alpha)-$proper (or circular) if it is invariant under two rotations [12], i.e.

$$q[n] = e^{\eta\theta_1} q[n] e^{\alpha\theta_2} \tag{37}$$

where the angles θ_1, θ_2 lie between $-\pi/2$ and $\pi/2$. For a more comprehensive analysis on properness, the reader is referred to [12]. Next, Section IV provides simulation examples to illustrate the relevance of quaternion statistics in 3D orientation/rotation applications. For clarity and conciseness, further theoretical considerations of properness are omitted in the next section.

This article has been accepted for publication in IEEE Signal Processing Magazine. This is the author's version which has not been fully edited and content may change prior to final publication. Citation information: DOI 10.1109/MSP.2024.3384178

IV. Making sense of quaternion statistics in 3D orientations

The aim of this section is to illustrate and demystify quaternion statistics. To this end, the usefulness of quaternions is first demonstrated in terms of tracking the statistics of trajectories on a 3D sphere. Second, the symmetries of the absolute values of autocorrelations (Property P4) are demonstrated. Third, the relationships between the different autocorrelations in Table II and Eq. (33) are elaborated visually. Figs. 1-4 show the *absolute* values of the autocorrelations in Eq. (12) for different trajectories, which were normalised by the total number of samples (i. e. 1,001 3D samples) for each example. To make sense of these quaternion autocorrelations $r[\ell]$ (the four top right plots), Figs. 1-4 also show the *real* autocorrelations $c[\ell]$ in the nine bottom plots.

This article has been accepted for publication in IEEE Signal Processing Magazine. This is the author's version which has not been fully edited and content may change prior to final publication. Citation information: DOI 10.1109/MSP.2024.3384178

Simulation 1. Fig. 1 shows an example of no particular trajectory (random walk) on a 3D sphere. From the top plots, it is clear that all quaternion autocorrelations vanish (except at the lag $\ell = 0$) to reflect the randomness of the 3D data. As such, at lag $\ell = 0$, we have

$$\begin{aligned} r_c[0] &= 0.000999 + 0\imath + 0\jmath + 0\kappa \\ r_p[0] &= -0.000999 + 0\imath + 0\jmath + 0\kappa \\ r_\imath[0] &= -0.00032707 + 0\imath + 0\jmath + 0\kappa \\ r_\jmath[0] &= -0.00035628 + 0\imath + 0\jmath + 0\kappa \\ r_\kappa[0] &= -0.00031565 + 0\imath + 0\jmath + 0\kappa \end{aligned} \tag{38}$$

Eq. (38) confirms the relationship $r_c[\ell] = -r_p[\ell]$ in Eq. (33). Moreover, plugging in the autocorrelation values in Eq. (38) into the relationship in Eq. (26) confirms the validity of the latter.

The observed lack of structure in terms of 3D trajectory implies that $r_\eta[\ell]$ follows the same pattern as $r_c[\ell]$. Moreover, $r_\eta[\ell]$ are real-valued, confirming the lack of correlation between each $\perp$ coordinate due to the randomness of the data. This is confirmed in the bottom plots of the six real (cross) autocorrelation such as $c_{12}[\ell], c_{13}[\ell], c_{23}[\ell]$. On the other hand, $r_c[0]$ and $r_p[0]$ are by definition real-valued at lag $\ell = 0$ and maximum just like the three real autocorrelations $c_{11}[\ell], c_{22}[\ell], c_{33}[\ell]$.

This article has been accepted for publication in IEEE Signal Processing Magazine. This is the author's version which has not been fully edited and content may change prior to final publication. Citation information: DOI 10.1109/MSP.2024.3384178

Simulation 2. Fig. 2 shows an example of a 3D oblique trajectory that involves non-zero coordinates on all three $\perp$ axes. Considering the lag $\ell = 0$, we have

$$\begin{aligned} r_c[0] &= 0.000999 + 0\imath + 0\jmath + 0\kappa \\ r_p[0] &= -0.000999 + 0\imath + 0\jmath + 0\kappa \\ r_\imath[0] &= 0.00019605 + 0\imath - 0.00013661\jmath + 0.0001351\kappa \\ r_\jmath[0] &= -0.00034437 + 0.00030387\imath + 0\jmath - 0.0001351\kappa \\ r_\kappa[0] &= -0.00085068 - 0.00030387\imath + 0.00013661\jmath + 0\kappa \end{aligned} \tag{39}$$

Unlike Simulation 1, $r_\eta[\ell]$ are not constrained to real values due to the correlation between the three imaginary components - which is confirmed by the real (cross) autocorrelations, e.g. $c_{12}[\ell]$,$c_{23}[\ell]$, $c_{31}[\ell]$. Fig. 2 shows four different patterns, although only three of these are distinct in shape from one another. In fact, the autocorrelations $|r_c[\ell]|$, $|r_p[\ell]|$ are *approximately* equal to $|r_\kappa[\ell]|$ in magnitude. The three distinct patterns exhibited by $r_c[\ell]$, $r_\imath[\ell]$, and $r_\jmath[\ell]$ in Fig. 2 suggest that these three statistical descriptors are sufficient to describe the complete second order information of the 3D trajectory in Simulation 2. This can be verified by using Eq. (34) to calculate the last unknown autocorrelation $r_\kappa[\ell]$ - this is also confirmed by the values of the autocorrelations in Eq. (39). The maximum value of $c_{23}[\ell]$ at lag $\ell = 0$ indicates that the activities in the y-axis z-axis are more synchronised than with the activity in x-axis. This synchronisation is reflected by the maximum values at $\ell = 0$ for the corresponding quaternion counterparts $r_\kappa[\ell]$ and $r_\jmath[\ell]$.

Simulation 3. Fig. 3 shows an example of a horizontal trajectory on a 3D sphere that involves non-zero coordinates in the x and y axes only. Considering the lag $\ell = 500$, we have

$$\begin{aligned} r_c[500] &= 0 + 0\imath + 0\jmath + 0.0005\kappa \\ r_p[500] &= 0 + 0\imath + 0\jmath - 0.0005\kappa \\ r_\imath[500] &= -0.00031767 + 0\imath + 0\jmath + 0\kappa \\ r_\jmath[500] &= 0.00031767 + 0\imath + 0\jmath + 0\kappa \\ r_\kappa[500] &= 0 + 0\imath + 0\jmath - 0.0005\kappa \end{aligned} \tag{40}$$

Similarly to the previous simulations, Eq. (40) confirms the relationship $r_\imath[\ell] = -r_\jmath[\ell]$ and $r_c[\ell] = -r_\kappa[\ell]$ in Table II. Moreover, plugging in the values in Eq. (40) into the relationship Eq. (34) confirms the validity of the latter.

Observe that the lag $\ell \neq 0$ considered in Eq. (40) implies that both the imaginary parts $\Im\{r_c[500]\}, \Im\{r_p[500]\} \neq 0$. Moreover, since there is no activity in the z-axis, the autocorrelation $r_\kappa[500]$ does not bring any new information when compared to $r_c[500]$ and $r_p[500]$, since $|r_\kappa[\ell]| = |r_c[\ell]| = |r_p[\ell]|$. The inactivity in the z-axis is confirmed by the bottom plots of the real (vanishing) autorrelation of the third channel, e.g. $c_{33}[\ell] = c_{23}[\ell] = c_{13}[\ell] = 0$, which are redundant statistics like its quaternion counterpart $|r_\kappa[\ell]|$.

Simulation 4. Fig. 4 shows an example of a vertical trajectory in the X plane that involves non-zero coordinates in the x and z axes only. Considering the lag $\ell = 500$, we have

$$\begin{aligned} r_c[500] &= 0 + 0\imath + 0.0005\jmath + 0\kappa \\ r_p[500] &= 0 + 0\imath - 0.0005\jmath + 0\kappa \\ r_\imath[500] &= -0.00031767 + 0\imath + 0\jmath + 0\kappa \\ r_\jmath[500] &= 0 + 0\imath - 0.0005\jmath + 0\kappa \\ r_\kappa[500] &= 0.00031767 + 0\imath + 0\jmath + 0\kappa \end{aligned} \tag{41}$$

Like in Simulation 3, the imaginary parts $\Im\{r_c[500]\}, \Im\{r_p[500]\} \neq 0$ due to the non-zero lag. Note the redundancy of the autocorrelation $r_\jmath[\ell]$, as the trajectory does not reside in the y-axis, leading to $|r_\jmath[\ell]| = |r_c[\ell]| = |r_p[\ell]|$. This redundancy is also reflected by the vanishing real autocorrelations of the second channel, i.e. $c_{22}[\ell] = c_{21}[\ell] = c_{23}[\ell] = 0$.

Observe also that Eq. (41) confirms the relationship $r_\imath[\ell] = -r_\kappa[\ell]$ and $r_c[\ell] = -r_\jmath[\ell]$ in Table II. Moreover, plugging in the values in Eq. (41) into the relationship in Eq. (34) confirms the validity of the latter.

Although these simulations illustrate different trajectories, their statistics share the following similar traits as observed from Figs. 1-4:

- T1 The symmetries of the autocorrelations $|r[\ell]| = |r[-\ell]|$ along the y axis (at the lag $\ell = 0$), confirming Property P4;
- T2 The equalities of the autocorrelations $|r_c[\ell]| = |r_p[\ell]|$, as governed by Eq. (33);
- T3 The equalities of the autocorrelation $|r_\eta[\ell]| = |r_c[\ell]| = |r_p[\ell]|$ (as observed in **Remark 1**) when there is no activity in the corresponding axis of rotation. For example, in Simulation 3, the zero values in the z axis for the horizontal trajectory lead to the redundancy of $|r_\kappa[\ell] = |r_c[\ell]|$;
- T4 The maximum values of $|r_c[0]|$ and $|r_p[0]|$ at lag $\ell = 0$, due to property P2 and Eq. (33);
- T5 The maximum values of $|r_\eta[0]|$ at lag $\ell = 0$, if there is either a redundancy in

that axis or a lack of structure in the 3D trajectory due to randomisation.

In addition to these insights, the overarching contribution to this work is to demonstrate how quaternion statistics can be exploited to classify different 3D trajectories based on the redundancies of some autocorrelations. For instance, the redundancy of $|r_\kappa[\ell]|$ in Simulation 3 indicates that there is no activity in the z axis, hence a horizontal trajectory on the unit sphere. Likewise, the redundancy of $|r_\jmath[\ell]|$ indicates a vertical trajectory in the X plane (or no activity in the y axis) for Simulation 4. Now that the fundamentals of augmented statistics have been established, some applications of augmented statistics are next revisited, with a focus on 3D orientation applications.

V. Applications

Augmented statistics for quaternions have been considered in a range of applications including sleep analysis [26], renewable energy [27], and seismic data analysis [28]. Given that quaternions are best known for the modelling of 3D rotations, we next elaborate two applications of quaternion signal processing and augmented statistics in the context of 3D orientations. Application 1 is concerned with the tracking of the orientation variable $q[n]$ for an unmanned aerial vehicle, while Application 2 considers the denoising of the orientation variable $q[n]$ from a multiplicative noise. The algorithms considered were the Quaternion Least Mean Square[9] (QLMS) without augmented statistics, the widely linear QLMS with augmented statistics [30], and a benchmark algorithm tailored for each application. To facilitate reproducibility, these real-world applications were adopted from the examples provided by Mathworks. For more details, the readers are referred to the hyperlinks provided. Moreover, the Supplementary Material[10] at offer further practical insights to facilitate the adoption of augmented quaternion statistics in applications.

To illustrate how the QLMS and the widely QLMS algorithms differ in quaternion statistics, consider their weight updates. For QLMS, its weight update[11] can be

[9]A hardware QLMS implementation based on parallel processing can be found in [29].

[10]This paper has supplementary downloadable material available at http://ieeexplore.ieee.org., provided by the authors. Contact clive.cheongtook@rhul.ac.uk for further questions about this work.

[11]Based on the assumption that the output filter can be computed as $y[n] = \mathbf{w}^{\mathsf{H}}[n]\mathbf{q}[n]$.

expressed as:

$$\begin{aligned} \mathbf{w}[n+1] &= \mathbf{w}[n] + \mu \mathbf{q}[n] e^*[n] \\ \mathsf{E}\left\{\mathbf{w}[n+1]\right\} &= \mathsf{E}\left\{\mathbf{w}[n]\right\} + \mu \mathbf{R}[n] \mathsf{E}\left\{\mathbf{w}_{\mathrm{o}}[n] - \mathbf{w}[n]\right\} \end{aligned} \tag{42}$$

where $\mathbf{w}[n]$, $\mathbf{w}_{\mathrm{o}}[n]$, and $e[n]$ denote respectively the learnt weights, the optimal weights (in terms of minimum mean square error) and the error. Observe that QLMS exploits the covariance $\mathbf{R}[n]$ of the input $\mathbf{q}[n]$ only. On the other hand, the widely linear QLMS takes advantage of augmented statistics through the use of the augmented covariance $\mathbf{R}^a[n]$ within its update [30]:

$$\begin{aligned} \mathbf{w}^a[n+1] &= \mathbf{w}^a[n] + \mu \mathbf{q}^a[n] e^*[n] \\ \mathsf{E}\left\{\mathbf{w}^a[n+1]\right\} &= \mathsf{E}\left\{\mathbf{w}^a[n]\right\} + \mu \mathbf{R}^a[n] \mathsf{E}\left\{\mathbf{w}^a_{\mathrm{o}}[n] - \mathbf{w}^a[n]\right\} \end{aligned} \tag{43}$$

where the weight vectors $\mathbf{w}[n]$ and $\mathbf{w}_{\mathrm{o}}[n]$ have been augmented by four folds to $\mathbf{w}^a[n]$ and $\mathbf{w}^a_{\mathrm{o}}[n]$ for widely linear processing. Similarly, the statistics have been augmented to include not only the covariance $\mathbf{R}[n]$, but also the complementary covariances $\mathbf{R}_\imath[n]$, $\mathbf{R}_\jmath[n]$, and $\mathbf{R}_\kappa[n]$, i.e.

$$\mathbf{R}^a[n] = \mathsf{E}\left\{\mathbf{q}^a[n]\mathbf{q}^{a^{\mathsf{H}}}[n]\right\} = \begin{bmatrix} \mathbf{R}[n] & \mathbf{R}_\imath[n] & \mathbf{R}_\jmath[n] & \mathbf{R}_\kappa[n] \\ (\mathbf{R}_\imath[n])^\imath & (\mathbf{R}[n])^\imath & (\mathbf{R}_\kappa[n])^\imath & (\mathbf{R}_\jmath[n])^\imath \\ (\mathbf{R}_\jmath[n])^\jmath & (\mathbf{R}_\kappa[n])^\jmath & (\mathbf{R}[n])^\jmath & (\mathbf{R}_\imath[n])^\jmath \\ (\mathbf{R}_\kappa[n])^\kappa & (\mathbf{R}_\jmath[n])^\kappa & (\mathbf{R}_\imath[n])^\kappa & (\mathbf{R}[n])^\kappa \end{bmatrix} \tag{44}$$

owing to the *augmented* input $\mathbf{q}^a[n] = \Big[\mathbf{q}[n],\ \mathbf{q}^\imath[n],\ \mathbf{q}^\jmath[n],\ \mathbf{q}^\kappa[n]\Big]$. The complementary covariances $\mathbf{R}_\eta[n]$ can be further expanded into the structure in Eq. (29) made up of η-autocorrelations $r_\eta[\ell]$ as defined in Eq. (20). Similarly, the covariance $\mathbf{R}[n]$ matrix can be constructed with the building block of $r_c[\ell]$. For a horizontal motion such as in Simulation 3, the augmented input can be reduced to $\mathbf{q}^a[n] = \Big[\mathbf{q}[n],\ \mathbf{q}^\jmath[n]\Big]$, whereas for a vertical motion in the X plane in Simulation 4, a sufficient input corresponds to $\mathbf{q}^a[n] = \Big[\mathbf{q}[n],\ \mathbf{q}^\kappa[n]\Big]$. We refer to Table II to sufficient statistics for 2D modelling.

Application 1. Consider the tracking of 3D orientations of an unmanned aerial vehicle (UAV), which involves determining the orientation of $q[n]$ from its current position $p^{\dagger}[n]$ and its previous positions $p[n]$, as in Eq. (1). Fig. 5 shows a real-world example of tracking the 3D orientation of a UAV for a duration of approximately 18 seconds. This simulation was adapted from an example[b] on data fusion of IMU sensors (such as accelerometers and gyroscopes) with GPS sensors. The 3D orientation can be tracked 'live' by the 3D scope (like a virtual gyroscope) in the bottom right plot of Fig. 5. The actual position of the UAV involves not only rotation but also translation, which means that its movement extends beyond the unit sphere; this makes it difficult to visualise the rotational movements. To circumvent this visualisation issue, the left hand plot shows the position of the UAV, if it were to start at position $(1, 0, 0)$ on a unit sphere, and its subsequent movements were restricted to the actual orientations (rotations) of the UAV, whilst neglecting the translational movements. The top right plot of Fig. 5 tracks the errors of the widely linear Quaternion LMS (denoted as 'widely linear QLMS') based on augmented statistics, the strictly linear Quaternion LMS without augmented statistics (denoted as 'standard linear QLMS') [30], and the benchmark real-valued Kalman filter taken from the Mathworks example. The benchmark real-valued Kalman filter tracked well the orientations given that all its estimates were well within a margin error of one degree. However, the direct operation in $\mathbb{H}$ exhibited performance benefits, especially when augmented statistics were taken into account. In the context of augmented statistics, Property PI on $\eta-$Hermitian Toeplitz structure in Eq. (30) can be exploited to reduce the computational complexity of complementary correlation matrices $\mathbf{R}_{\eta}[n]$, since only τ entries of $\mathbf{R}_{\eta}[n]$ need to be calculated explicitly, instead of τ^2 entries. The same trick can be used for the computation of the Toeplitz covariance $\mathbf{R}_{c}[n]$.

[b] https://www.mathworks.com/help/fusion/ug/imu-and-gps-fusion-for-inertial-navigation.html

This article has been accepted for publication in IEEE Signal Processing Magazine. This is the author's version which has not been fully edited and content may change prior to final publication. Citation information: DOI 10.1109/MSP.2024.3384178

Application 2. Consider the denoising of the 3D orientation variable $q[n]$, where the nature of the noise is multiplicative as in Eq. (1), and of the same form as the orientation variable $q[n]$, i.e. a full quaternion variable. Consequently, the uncertainty associated with the new position $p^{\dagger}[n]$ in Eq. (1) due to the multiplicative noise $q_{\text{noise}}[n]$ can be modelled as

$$p^{\dagger}[n] = \Big(q_{\text{noise}}[n]q[n]\Big)p[n]\Big(q^{*}[n]q^{*}_{\text{noise}}[n]\Big) \tag{45}$$

This application was taken from an example[c] of Mathworks, which demonstrated the low pass filtering of 3D orientation $q[n]$ by a real-valued algorithm called spherical linear interpolation (SLERP), which is the best known algorithm in 3D rotations. Fig 6 compares the performance of the benchmark SLERP algorithm with the widely QLMS (with augmented statistics) and the strictly linear QLMS (without augmented statistics). All algorithms performed well given the proximities of their estimates with the ground truth 3D rotation in all the axes of rotation. The advantage of the SLERP is that it requires no teaching (or desired) signal, since it denoises the 3D orientation signal $q[n]$ by interpolating between two consecutive noisy samples. However, this benefit comes at the expense of weaker performance compared to the widely linear QLMS and strictly linear QLMS, as illustrated in the bottom plot in Fig. 6. The widely linear QLMS performed better than the standard QLMS, owing to the use of *augmented* statistics.

[c]https://www.mathworks.com/help/nav/ug/lowpass-filter-orientation-using-quaternion-slerp.html

VI. Conclusion

This tutorial embarks upon our foundation work on quaternion statistics [1] to establish a reader friendly insight and guide into their current and emerging applications. This has involved the statistical characterisation of quaternion sequences, properties of quaternion auto-correlations, and the degeneracy of quaternion correlations when considering 3D or 2D (complex) data. This has served to demonstrate how quaternion statistics can act as a lynchpin in machine learning algorithms in 3D and 4D. Whilst keeping focus on making sense from quaternion statistics and opening avenues for

further developments in this field, this paper also complements our sister paper [20], which revisits quaternion learning algorithms and their applications.

VII. Biographies

Clive Cheong Took (clive.cheongtook@rhul.ac.uk) received his doctorate from Cardiff University. He is a senior lecturer at Royal Holloway, University of London, U.K. He has been working on quaternion signal processing since 2008 and delivered a tutorial on this topic in the EUSIPCO 2011 conference. Some of his contributions to this area include augmented statistics, adaptive learning, and novel matrix factorisations.

Sayed Pouria Talebi (s.talebi12@alumni.imperial.ac.uk) received his doctorate degree from Imperial College London, where his research focused on quaternion-valued signal processing. He has also been a research fellow at NTNU in Norway and Aalto University in Finland. He has since served as an invited researcher at University of Cambridge and a Research Associate at King's College London. Some of his contributions to this area include formulation of the theory of quaternion-valued multi-agent systems, formulation of the basis of quaternion-valued control theory, and quaternion-valued nonlinear/non-Gaussian signal processing.

Rosa Maria Fernandez Alcala (rmfernan@ujaen.es) received her doctotal degree from University of Jaén, Spain. Rosa is an associate professor with the Department of Statistics and Operations Research, University of Jaén. Amongst her contributions includes the "widely linear estimation algorithms for second-order stationary signals" and she has a keen interest in proper hypercomplex signal processing as a dimension reduction technique.

Danilo Mandic (d.mandic@ic.ac.uk) received the Ph.D. degree in nonlinear adaptive signal processing in 1999 from Imperial College, London, where he is now a Professor. He specialises in Statistical Learning Theory, Machine Intelligence, and Statistical Signal Processing. He is the President of the International Neural Networks Society and a Distinguished Lecturer of both the IEEE Computational Intelligence Society and the IEEE Signal Processing Society.

REFERENCES

[1] C. Cheong Took and D. P. Mandic, "Augmented second-order statistics of quaternion random signals," *Signal Processing*, vol. 91, no. 2, pp. 214–224, 2011.

[2] W. R. Hamilton, "On quaternions, or on a new system of imaginaries in algebra," *Philosophical Magazine*, 1844–1850.

[3] C. Smith and M. N. Wise, *Energy and Empire: A Biographical Study of Lord Kelvin*. Cambridge University Pres, 1892.

[4] O. Heaviside, "Vectors versus quaternions," *Nature*, vol. 47, p. 533–534, 1893.

[5] C. Pritchard, "Tendril of the hop and tendril of the vine: Peter guthrie tait and the promotion of quaternions, part i," *The Mathematical Gazette*, vol. 82, no. 493, pp. 26–36, 1998.

[6] J. Lambek, "If hamilton had prevailed: quaternions in physics," *The Mathematical Intelligencer*, vol. 17, pp. 7–15, 1995.

[7] S. Said, N. L. Bihan, and S. J. Sangwine, "Fast complexified quaternion Fourier transform," *IEEE Transactions on Signal Processing*, vol. 56, no. 4, pp. 1522–1531, 2008.

[8] J. Navarro-Moreno, R. M. Fernandez-Alcala, and J. C. Ruiz-Molina, "A quaternion widely linear series expansion and its applications," *IEEE Signal Processing Letters*, vol. 19, no. 12, pp. 868–871, 2012.

[9] H. Li, H. Li, and L. Zhang, "Quaternion-based multiscale analysis for feature extraction of hyperspectral images," *IEEE Transactions on Signal Processing*, vol. 67, no. 6, pp. 1418–1430, 2019.

[10] D. Rose, "Rotations in three-dimensions: Euler angles and rotation matrices," *Engineering Notes*, 2015.

[11] N. N. Vakhania, "Random vectors with values in quaternion hilbert spaces," *Theory of Probability & Its Applications*, vol. 43, no. 1, pp. 99–115, 1999.

[12] S. Miron, J. Flamant, N. L. Bihan, P. Chainais, and D. Brie, "Quaternions in signal and image processing: A comprehensive and objective overview," *IEEE Signal Processing Magazine*, vol. 40, no. 6, pp. 26–40, 2023.

[13] J. Vía, D. Ramírez, and I. Santamaría, "Properness and widely linear processing of quaternion random vectors," *IEEE Transactions on Information Theory*, vol. 56, no. 7, pp. 3502–3515, 2010.

[14] P. Ginzberg and A. T. Walden, "Testing for quaternion propriety," *IEEE Transactions on Signal Processing*, vol. 59, no. 7, pp. 3025–3034, 2011.

[15] E. Grassucci, D. Comminiello, and A. Uncini, "A quaternion-valued variational autoencoder," in *IEEE International Conference on Acoustics, Speech and Signal Processing (ICASSP)*, pp. 3310–3314, 2021.

[16] E. Grassucci, E. Cicero, and D. Comminiello, *Quaternion Generative Adversarial Networks*, pp. 57–86. Cham: Springer International Publishing, 2022.

[17] T. K. Paul and T. Ogunfunmi, "A kernel adaptive algorithm for quaternion-valued inputs," *IEEE Transactions on Neural Networks and Learning Systems*, vol. 26, no. 10, pp. 2422–2439, 2015.

[18] T. Parcollet, M. Morchid, and G. Linarès, "A survey of quaternion neural networks," *Artificial Intelligence Review*, vol. 53, p. 2957–2982, 2020.

[19] C. Cheong Took, D. P. Mandic, and F. Zhang, "On the unitary diagonalisation of a special class of quaternion matrices," *Applied Mathematics Letters*, vol. 24, no. 11, pp. 1806–1809, 2011.

[20] D. P. Mandic, S. P. Talebi, C. Cheong Took, Y. Xia, D. Xu, and P. Bourigault, "The $\mathbb{HR}$-calculus: Enabling information processing with quaternion algebra," *arXiv:2311.16771*, 2023.

[21] J. Voight, *Quaternion Algebras*. Springer, 2021.

[22] S. Enshaeifar, C. Cheong Took, S. Sanei, and D. P. Mandic, "Novel quaternion matrix factorisations," in *Proceedings of the IEEE International Conference on Acoustics, Speech and Signal Processing (ICASSP)*, pp. 3946–3950, 2016.

[23] Y. Kim, J. Ryu, K. K. Kim, C. Cheong Took, D. P. Mandic, and C. Park, "Motor imagery classification using mu and beta rhythms of EEG with strong uncorrelating transform based complex common spatial patterns," *Computational Intelligence and Neuroscience*, no. 1489692, pp. 868–871, 2016.

[24] M. Xiang, S. Enshaeifar, A. E. Stott, C. Cheong Took, Y. Xia, S. Kanna, and D. P. Mandic, "Simultaneous diagonalisation of the covariance and complementary covariance matrices in quaternion widely linear signal processing," *Signal Processing*, vol. 148, pp. 193–204, 2018.

[25] S. Sangwine and N. L. Bihan, "Quaternion Toolbox for Matlab [Online]," *Available: http://qtfm.sourceforge.net/*, July 2005.

[26] Z. Huang and B. W.-K. Ling, "Sleeping stage classification based on joint quaternion valued singular spectrum analysis and ensemble empirical mode decomposition," *Biomedical Signal Processing and Control*, vol. 71, p. 103086, 2022.

[27] C. Cheong Took, G. Strbac, K. Aihara, and D. Mandic, "Quaternion-valued short-term joint forecasting of three-dimensional wind and atmospheric parameters," *Renewable Energy*, vol. 36, no. 6, pp. 1754–1760, 2011.

[28] B. Brahia and M. D. Sacchi, "Quaternionic rank-reduction methods for vector-field seismic data processing," *Digital Signal Processing*, vol. 87, pp. 178–189, 2019.

[29] A. Tisan and C. Cheong Took, "Reconfigurable quaternion LMS," *IEEE Transactions on Industrial Informatics*, vol. 20, no. 3, pp. 4982–4989, 2024.

[30] C. Cheong Took, C. Jahanchahi, and D. P. Mandic, "A unifying framework for the analysis of quaternion valued adaptive filters," in *Conference Record of the Forty Fifth Asilomar Conference on Signals, Systems and Computers (ASILOMAR)*, pp. 1771–1774, 2011.

This article has been accepted for publication in IEEE Signal Processing Magazine. This is the author's version which has not been fully edited and content may change prior to final publication. Citation information: DOI 10.1109/MSP.2024.3384178

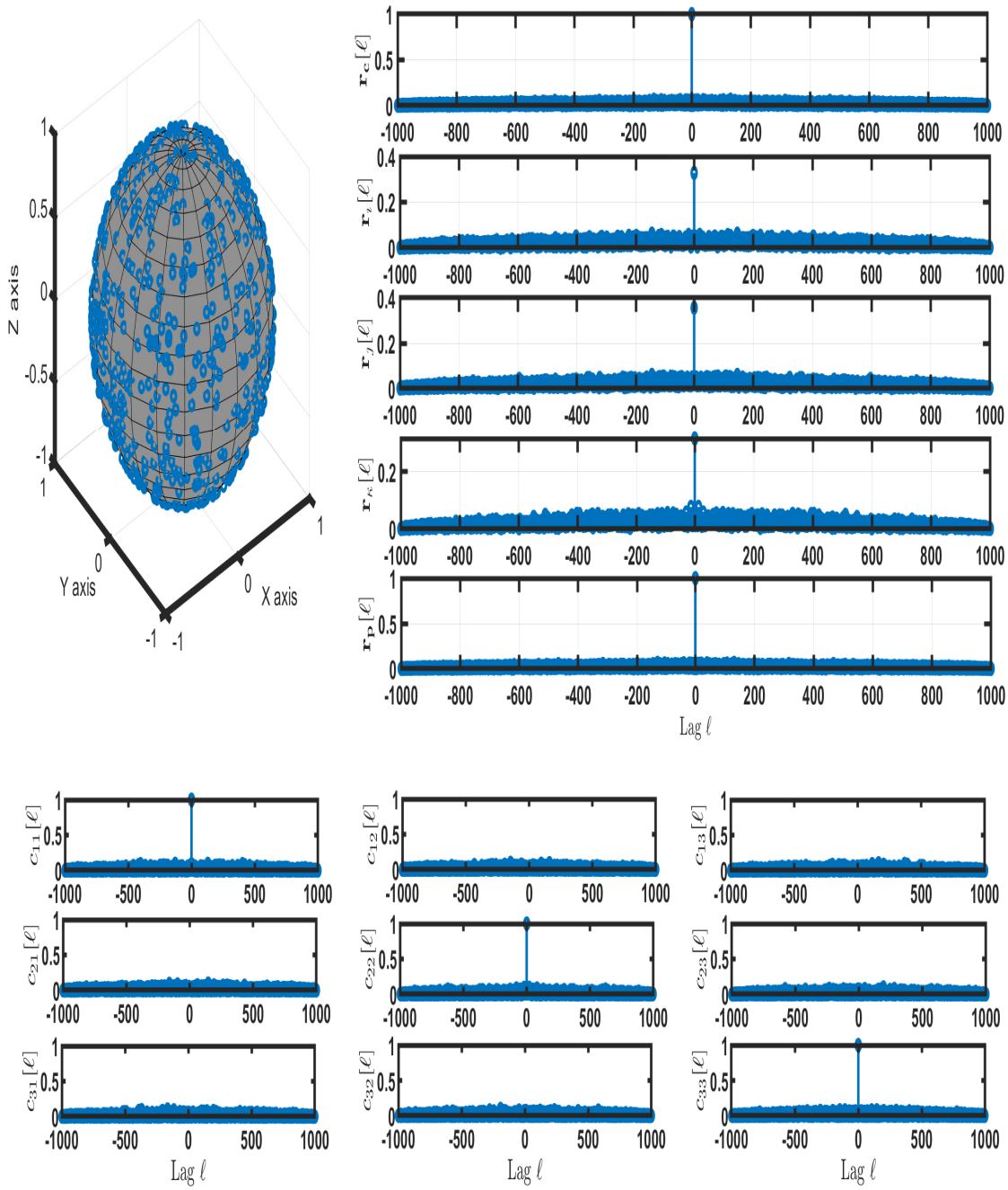

Fig. 1: Augmented quaternion statistics of no particular trajectory. Top Left: Random points on a unit sphere. Top Right: The vanishing auto-correlations (except at lag $\ell = 0$) indicate the randomness of the data. Bottom: 9 Real valued autocorrelations for trivariate signals.

This article has been accepted for publication in IEEE Signal Processing Magazine. This is the author's version which has not been fully edited and content may change prior to final publication. Citation information: DOI 10.1109/MSP.2024.3384178

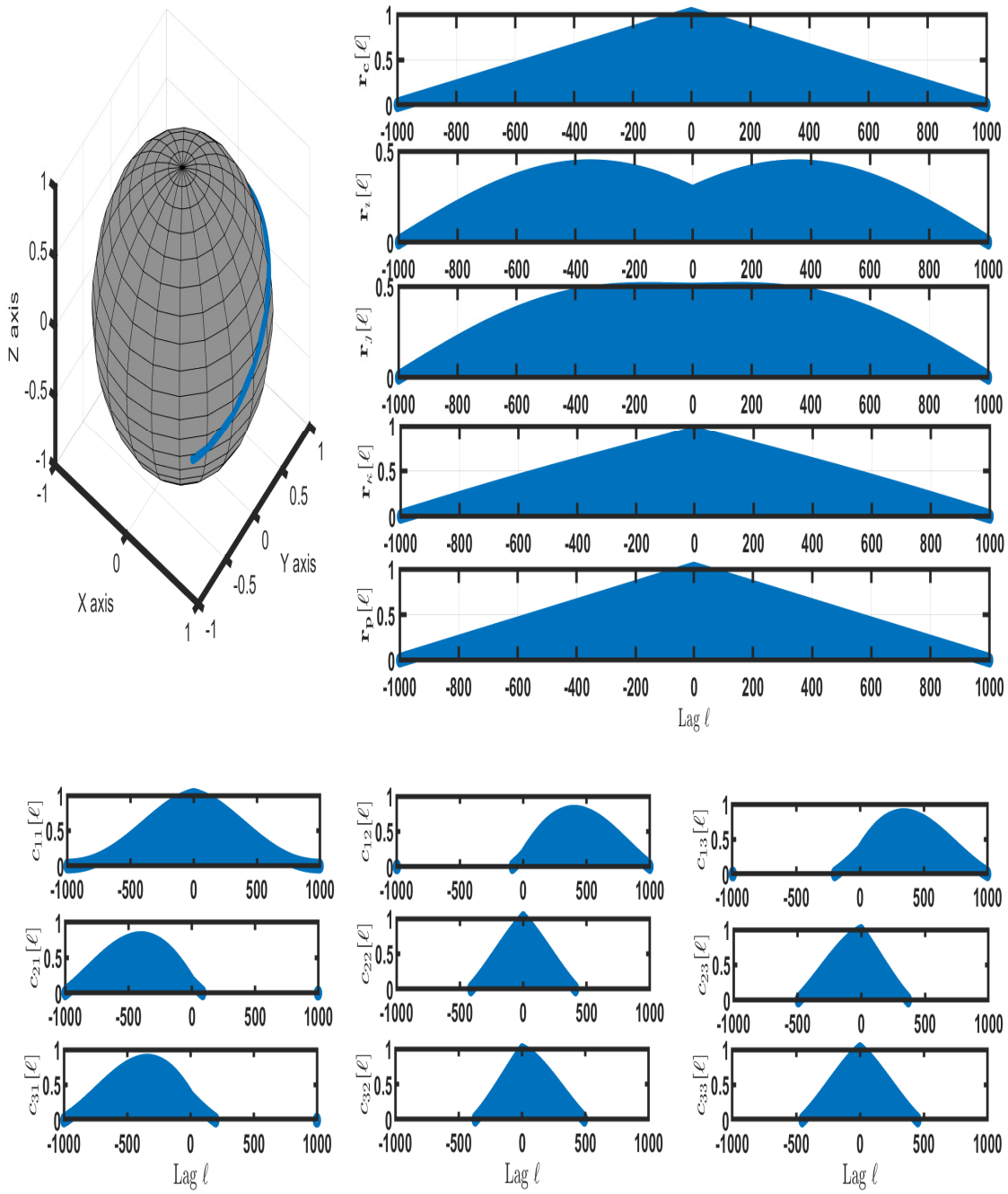

Fig. 2: Augmented quaternion statistics of a 3D trajectory. Top Left: A 3D oblique trajectory on a unit sphere. Top Right: Only three distinct patterns are exhibited by the auto-correlations, illustrating that only three descriptors are sufficient, e.g. $r_c[\ell]$, $r_i[\ell]$ and $r_j[\ell]$. Note, however, that $|r_k[\ell]| \neq |r_c[\ell]|$ in this example, despite their similarity. Bottom: 9 Real valued autocorrelations for trivariate signals.

This article has been accepted for publication in IEEE Signal Processing Magazine. This is the author's version which has not been fully edited and content may change prior to final publication. Citation information: DOI 10.1109/MSP.2024.3384178

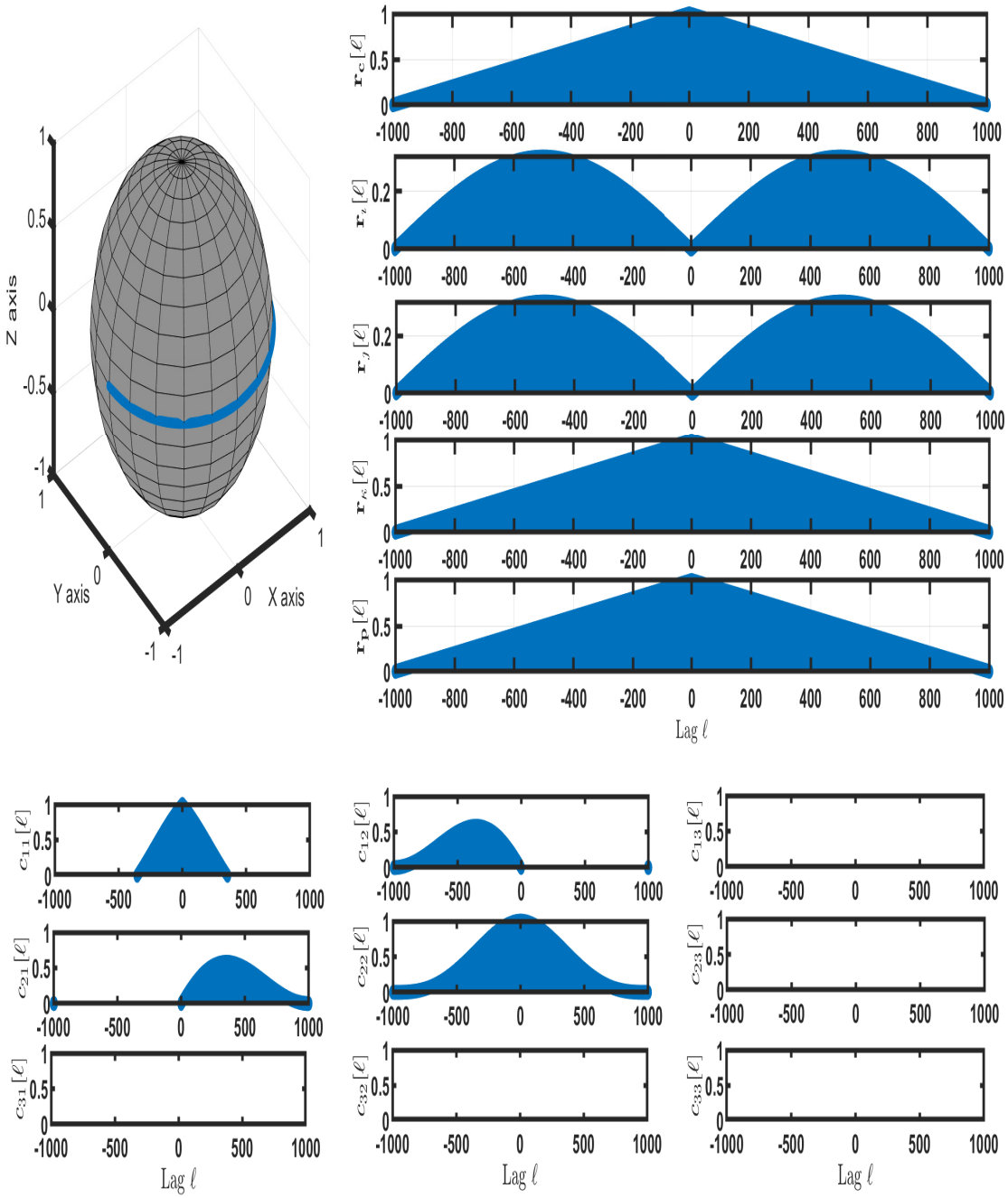

Fig. 3: Augmented quaternion statistics of a 2D trajectory. Top Left: A 2D horizontal trajectory on a unit sphere. Top Right: Only two distinct patterns are exhibited by the auto-correlations, illustrating that only two descriptors are sufficient, e.g. $r_c[\ell]$ and $r_\jmath[\ell]$. Bottom: 9 Real valued autocorrelations for trivariate signals.

This article has been accepted for publication in IEEE Signal Processing Magazine. This is the author's version which has not been fully edited and content may change prior to final publication. Citation information: DOI 10.1109/MSP.2024.3384178

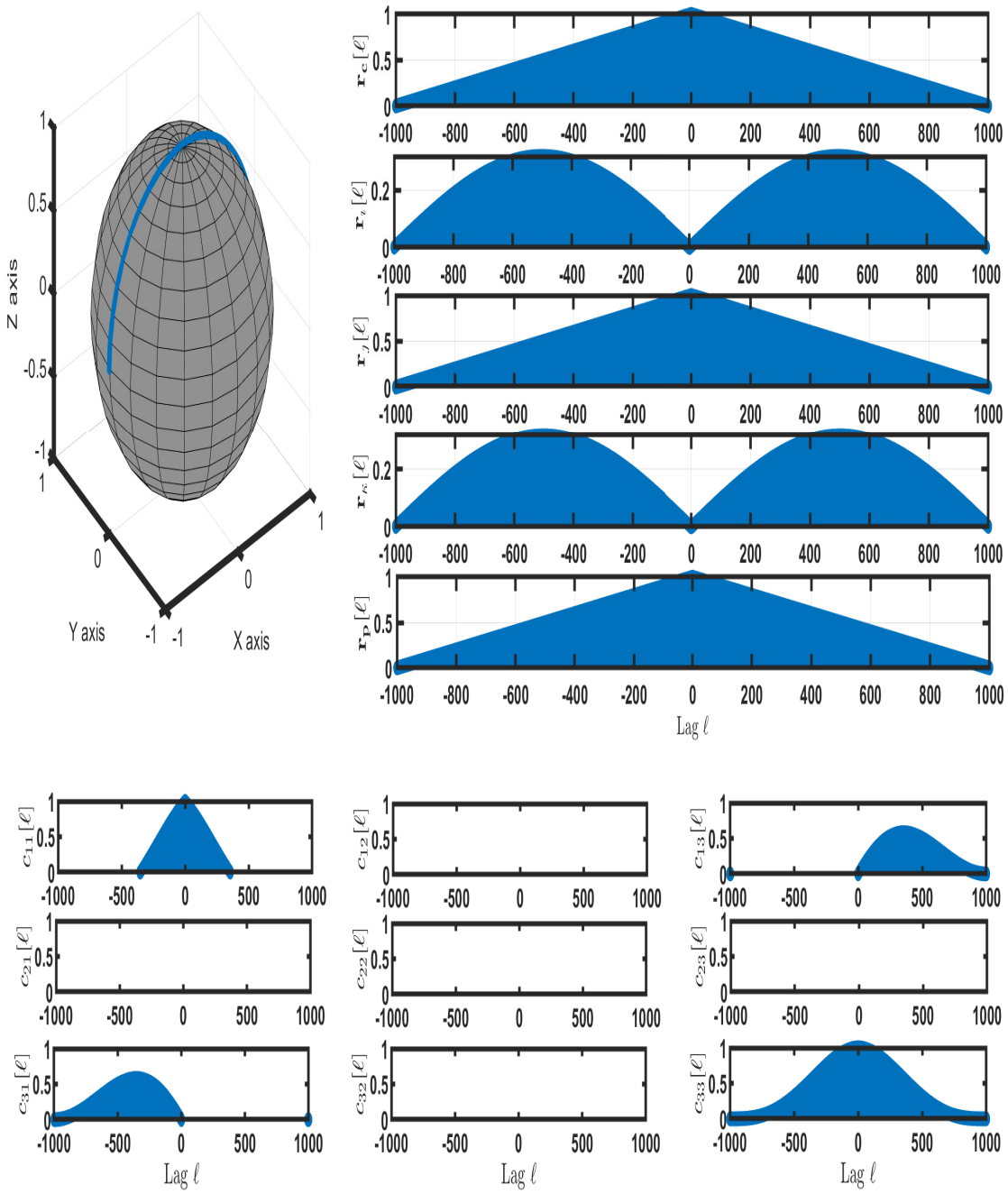

Fig. 4: Augmented quaternion statistics of a 2D trajectory. Top Left: a 2D vertical trajectory in X plane on a unit sphere. Top Right: Only two distinct patterns are exhibited by the auto-correlations, illustrating that two descriptors are sufficient, e.g. $r_c[\ell]$ and $r_i[\ell]$. Bottom: 9 Real valued autocorrelations for trivariate signals.

This article has been accepted for publication in IEEE Signal Processing Magazine. This is the author's version which has not been fully edited and content may change prior to final publication. Citation information: DOI 10.1109/MSP.2024.3384178

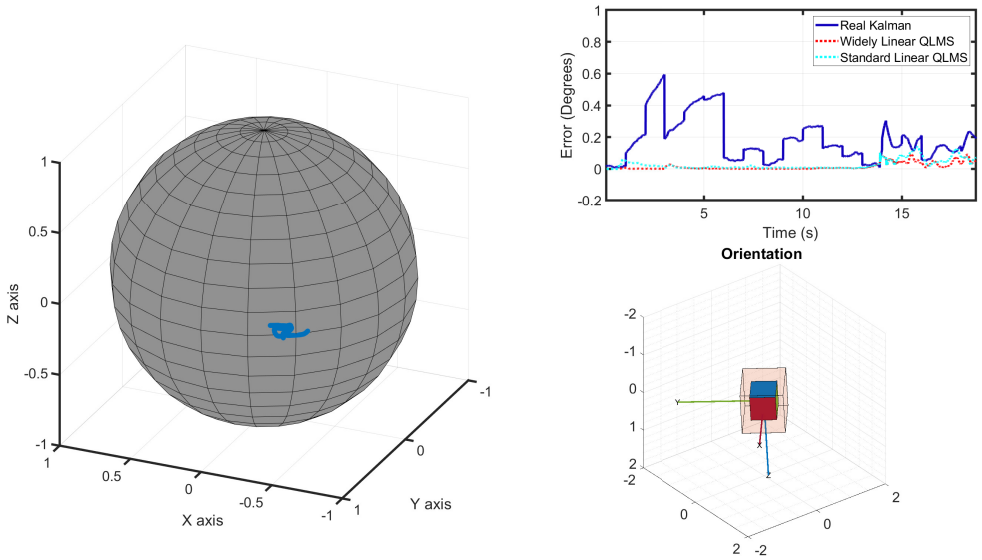

Fig. 5: Tracking the 3D orientation of a real-world unmanned aerial vehicle (UAV). Left: The plot displays the 3D positions of the UAV on a unit sphere, after the removal of translational motions. Right: The top plot shows the tracking errors of the benchmark real Kalman filter and the considered quaternion algorithms, i.e. the widely linear QLMS (augmented statistics) and the strictly (standard) linear QLMS (without augmented statistics). The bottom plot shows the 'live' scope that changes its 3D position according to the tracked orientation.

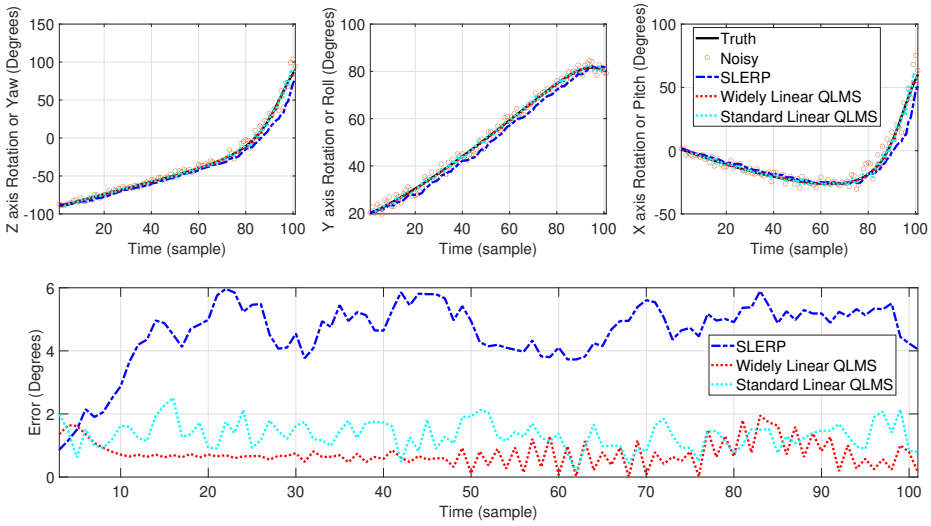

Fig. 6: Filtering of rotational (and multiplicative) noise in 3D orientation by the widely linear QLMS, the strictly (standard) linear QLMS, and the benchmark SLERP algorithm, a popular algorithm for the 'spherical' linear interpolation of 3D rotations.

VIII. Acknowledgement

We gratefully acknowledge the valuable feedback received from the anonymous reviewers. This work is sponsored by the I+D+i project PID2021-124486NB-I00, funded by Ministry of Science and Innovation, Spain (MCIN/AEI/10.13039/501100011033).